ORIGINAL RESEARCH

Comparative in vitro and in vivo Evaluation of Different Iron Oxide-Based Contrast Agents to Promote Clinical Translation in Compliance with Patient Safety

Harald Unterweger [1],*, Christina Janko [1],*, Tamara Folk[1], Iwona Cicha [1], Noémi Kovács[2], Gyula Gyebnár[3], Ildikó Horváth[4], Domokos Máthé [2,3], Kang H Zheng[5], Bram F Coolen[6], Erik Stroes[5], János Szebeni[7,8], Christoph Alexiou [1], László Dézsi [7,8,*], Stefan Lyer [1],*

[1]ENT-Department, Section of Experimental Oncology und Nanomedicine (SEON), Universitätsklinikum Erlangen, Erlangen, Germany; [2]Hungarian Centre of Excellence for Molecular Medicine, Semmelweis University, Budapest, Hungary; [3]Medical Imaging Centre, Semmelweis University, Budapest, Hungary; [4]Department Biophysics and Radiation Biology, Semmelweis University, Budapest, Hungary; [5]Department of Vascular Medicine, Amsterdam University Medical Centers, Amsterdam Cardiovascular Sciences, University of Amsterdam, Amsterdam, the Netherlands; [6]Department of Biomedical Engineering and Physics, Amsterdam University Medical Centers, Amsterdam Cardiovascular Sciences, University of Amsterdam, Amsterdam, the Netherlands; [7]Nanomedicine Research and Education Center, Institute of Translational Medicine, Semmelweis University, Budapest, Hungary; [8]SeroScience Ltd, Budapest, Hungary

*These authors contributed equally to this work

Correspondence: Harald Unterweger, Universitätsklinikum Erlangen, Glueckstr. 10a, Erlangen, 91054, Germany, Tel +49 9131 85-33142, Fax +49 9131 85-34828, Email harald.unterweger@uk-erlangen.de

Introduction: One of the major challenges in the clinical translation of nanoparticles is the development of formulations combining favorable efficacy and optimal safety. In the past, iron oxide nanoparticles have been introduced as an alternative for gadolinium-containing contrast agents; however, candidates available at the time were not free from adverse effects.
Methods: Following the development of a potent iron oxide-based contrast agent SPION^{Dex}, we now performed a systematic comparison of this formulation with the conventional contrast agent ferucarbotran and with ferumoxytol, taking into consideration their physicochemical characteristics, bio- and hemocompatibility in vitro and in vivo, as well as their liver imaging properties in rats.
Results: The results demonstrated superior in vitro cyto-, hemo- and immunocompatibility of SPION^{Dex} in comparison to the other two formulations. Intravenous administration of ferucarbotran or ferumoxytol induced strong complement activation-related pseudoallergy in pigs. In contrast, SPION^{Dex} did not elicit any hypersensitivity reactions in the experimental animals. In a rat model, comparable liver imaging properties, but a faster clearance was demonstrated for SPION^{Dex}.
Conclusion: The results indicate that SPION^{Dex} possess an exceptional safety compared to the other two formulations, making them a promising candidate for further clinical translation.
Keywords: magnetic resonance imaging, MRI, nanomedicine, nanoparticles, complement activation, CARPA

Introduction

Imaging the structure and function of tissues and organs is often the key to reliable medical diagnosis and a prerequisite for effective treatment. One of the most important imaging modalities in this regard is magnetic resonance imaging (MRI) which utilizes magnetic fields to excite protons, sparing the patients the exposure to ionizing radiation. It shows good local resolution and soft tissue contrast already in its native form. Nevertheless, the use of MRI contrast agents is often required for early detection of various diseases by strongly enhancing signal contrast between healthy and non-healthy tissue. Despite the widespread use of gadolinium-based contrast agents (GBCAs), the current gold standard, they produce side effects, which include allergic and adverse reactions, but can also lead to nephrogenic systemic fibrosis in

patients with renal failure.[1,2] In 2014, Kanda et al were the first to report the deposition of GBCAs in the deep nuclei of the brain[3] and multiple studies confirmed their findings afterwards.[4,5] There is also evidence that GBCA deposition can occur in children.[6] In a detailed review from 2017, Gulani et al summarized various studies on this topic and compared different gadolinium-based compounds.[7] Their findings suggest that linear GBCAs show a higher retention capacity in the brain compared to macrocyclic GBCAs; however, the current data are not sufficient to claim whether a clinical implication is necessarily associated with this deposition. As a result of these developments, both the US Food & Drug Administration (FDA)[8] and the European Medicines Agency (EMA)[9] have issued warnings against the use of GBCAs and recommended suspension of some linear agents/formulations. While the exact relationships between gadolinium deposition in the body and clinical implications are the subject of current investigations, alternatives to GBCAs are being sought and explored. In this context, superparamagnetic iron oxide nanoparticles (SPIONs) currently represent an interesting alternative contrast agent. Having strong magnetic susceptibility effects resulting in increased T_2 and T_2* related signal attenuation, they usually produce negative contrast with respect to healthy tissue, but under specific conditions positive/bright contrast is also feasible.[10] The strong signal decay associated with the presence of SPIONs makes them detectable in relatively low concentrations and therefore allow an increase in MRI sensitivity almost to the cellular level, as well as enable in vivo cell visualization and tracking.[11–13] Previously, only two SPION-based intravenous agents were clinically approved, namely ferumoxide (trade names: Feridex®, Endorem®) and ferucarbotran (trade name: Resovist®), but both were withdrawn from the market, mainly due to economic reasons. Nevertheless, Resovist®, available in Japan, is still commonly used as benchmark for new imaging techniques and devices.[14–18] Currently, however, there is a growing interest in the use of ferumoxytol (trade names: Rienso®, Feraheme®) as a SPION-based contrast agent for MRI. Ferumoxytol is indicated only as an intravenous iron replacement drug in adult patients with iron deficiency anemia, in particular those with chronic kidney disease or renal failure,[19,20] but is being used off-label for MRI.[21–23] The number of clinical trials using ferumoxytol either as a replacement for GBCAs or for completely new imaging modalities is steadily increasing. For example, in a retrospective study, ferumoxytol was shown to provide an equivalent assessment of the extent of bone and soft tissue sarcomas compared with GBCA.[24] It was also shown that ferumoxytol is equivalent to GBCA for the detection of intracranial metastases and could be a suitable alternative, especially when GBCAs are contraindicated.[25] Other example applications of ferumoxytol in MRI include the visualization of neurological features,[26,27] of acute kidney allograft rejection in pediatric patients,[28] or of myocardial hypoperfusion.[28]

Despite the promising clinical results, there are studies showing that SPION-based contrast agents can lead to considerable side effects. For example, administration of ferumoxide or ferucarbotran was associated with adverse events in 10% and 7.1% of all cases, respectively.[29] For ferucarbotran, there is also evidence that it can negatively affect autoimmune-mediated neuroinflammation after a single exposure.[30] A multicenter study carried out between 2003 and 2018 showed that ferumoxytol also tends to cause mostly mild side effects in 1.8% and moderate side effects in 0.2% of the patients, including hypertension, nausea, backache, headache, and vomiting.[31] However, cases of acute hypersensitivity were also reported. For this reason, ferumoxytol received the FDA's strongest type of warning in 2015, due to serious risk of potentially fatal anaphylactic reactions upon administration. The use of ferumoxytol for imaging may therefore pose a considerable risk to the patients.[32] Altogether, this calls for a SPION-based system with even better biocompatibility and a more comfortable diagnostic regimen for the patient. In our previous studies, we developed a nanoparticulate system named SPION^{Dex}, a type of SPIONs coated with crosslinked dextran, that fulfills these requirements.[33,34] These particles can be easily and reproducibly tuned in size and be stored for several months without any sign of agglomeration or sedimentation.[34] In vitro and in vivo results have also indicated that SPION^{Dex} represent an extremely biocompatible and non-immunogenic system, yet their direct comparison with ferucarbotran and ferumoxytol has not been reported so far. The current study thus aims at a systematic in vitro and in vivo comparison between the iron oxide-based nanosystems that can serve as MRI contrast agents in terms of biocompatibility and imaging performance, in order to evaluate their risk-to-benefit profile and the potential advantages of SPION^{Dex} in the clinical application.

Materials and Methods

Preparation of Nanoparticulate Contrast Agents

SPION^{Dex} were produced according to a modified protocol that was previously published.[33] In short, ferric and ferrous chloride salts were dissolved in a 10% (w/w) aqueous dextran solution at a molar Fe^{3+}:Fe^{2+} ratio of 2:1. The solution was cooled to 4 °C and dextran-coated iron oxide particles were precipitated with ammonia. After heating to 75 °C and subsequent cooling to room temperature, excess educts and byproducts were removed via tangential flow filtration (TFF; Repligen, USA) using a hollow fiber PES membrane (cut-off: 100 kDa). Next, sodium hydroxide was added to the particles and the dextran shell was crosslinked with epichlorohydrin. Eventually, the product was again washed via TFF, sterile filtered (0.2 μm) and stored at 4 °C until further use. All synthesis reagents were purchased from Merck, Germany, and are of Ph Eur purity were available, otherwise of *purum* quality. Resovist$^{®}$ was obtained from Schering Deutschland GmbH (Berlin, Germany) and Feraheme$^{®}$ from AMAG Pharmaceuticals (Waltham, USA).

Physicochemical Characterization of Nanoparticles

The iron concentration of the particles was determined via microwave plasma atomic emission spectroscopy (MP-AES; MP-4200 from Agilent Technologies, USA), using a commercially available iron standard solution (Bernd Kraft, Germany). The hydrodynamic size distributions, polydispersity indices and ζ-potentials at pH 7.4 were determined with a Malvern Nano ZS (United Kingdom) in backscattering mode. Thermogravimetric analysis was performed with freeze-dried nanoparticles using a TG 209 Libra (Netzsch, Germany). Fourier transform infrared spectroscopy (FTIR, ALPHA from Bruker, USA) was used to compare the different particle coatings. The magnetic behavior was investigated by measuring the magnetic volume susceptibility with a MS3/MS2G susceptometer (Bartington, United Kingdom). The MRI properties of the different iron oxide-based contrast agents were investigated with a 3 T Philips Ingenia MRI system (Netherlands). Thereby, T_1, T_2 and T_2* maps were scanned at different iron concentrations c_{np} and the images were processed using the VivoQuant 1.22 pre-clinical software (USA). The respective relaxivities r_i were derived from the relaxation rates R_i using the following equation[35]:

$$R_i = \frac{1}{T_i} = r_i \times c_{np} + R_d \tag{1}$$

where i reflects the scan mode (1 for T_1 and so on), T_i stands for the relaxation time and R_d is the diamagnetic relaxation rate of the dispersion medium.

Three independent experiments were performed with triplicate samples, and the results were averaged.

Examination of in vitro Cytocompatibility

The non-adherent, human T-cell leukemia cell line Jurkat (ACC 282, German Collection of Microorganisms and Cell Cultures GmbH, Germany) was used for the examination of the cytocompatibility. The cells were cultivated with RPMI 1640 medium supplemented with 10 vol% fetal bovine serum (FBS) and 1 vol% glutamine, in a cell culture incubator (INCOmed, Memmert, Germany) at 37 °C, 95% humidified air, and 5% CO_2. 2.5×10^5 Jurkat cells were seeded into each well of a 48 well plate and treated with different iron oxide-based contrast agents at a concentration range between 25 and 400 μg Fe/mL. Water served as negative control and 2% DMSO served as positive control. Every sample was prepared in triplicate. After incubation for 24 and 48 h, aliquots were stained with a freshly prepared staining solution containing AnnexinA5-FITC (AxV), Hoechst 33342 (Hoe), Hexamethylindodicarbo-cyanine iodide dye (DiI), and propidium iodide (PI).[36] In addition, the cell cycle and DNA degradation were investigated using propidium iodide staining in the presence of Triton X-100 (PIT).[37] In both cases, cell staining was examined via flow cytometry using a Gallios cytofluorometer (Beckman Coulter, USA). AxV is excited at 488 nm and recorded at 525/38 nm band pass (BP), PI is excited at 488 nm as well, but recorded at 620/30 nm BP, and Hoe is excited at 405 nm and recorded at 430/40 nm BP. Electronic compensation was used in order to eliminate any fluorescence bleed-through. Similarly, potential occurrence of iron induced reactive oxygen species (ROS) and the level of reduced glutathione were investigated using the fluorescent dyes 2'-7'dichlorofluorescin (DCFH) and monobromobimane (MBB), respectively.[38] Here, cells treated with 1 mM H_2O_2 served as positive control. Flow cytometry was performed to measure DCFH and MBB fluorescence

after 24 h of incubation with respective doses of contrast agents. In general, flow cytometry data were analyzed with Kaluza software 1.2 from Beckman Coulter (USA) and processed using Microsoft Excel (USA). All experiments were performed in triplicate, five times independently; the results were averaged.

In vitro Hemo- and Immunocompatibility

For hemocompatibility testing, blood was drawn from healthy volunteers. The use of human material was approved by the local ethics committee at the University Hospital Erlangen (# 257 14B) and the donors provided informed consent, in accordance with the Declaration of Helsinki. Colloidal stability of the nanoparticulate formulations in blood from three healthy volunteer donors was tested in the presence of three different anticoagulants, ie, lithium-heparin, ethylenedia-minetetraacetic acid (EDTA), and sodium citrate. 30 min after incubation, blood smears were prepared on glass slides and examined for nanoparticle agglomerates (>200 nm) by transmission light microscopy.

Hemolytic properties: The hemoglobin content of lithium-heparin-anticoagulated whole blood was adjusted to 5 mg/ mL in phosphate buffered saline (PBS). Nanoparticles were diluted in H_2O and incubated with the diluted blood for 3 h at 37 °C (ratio 1:10) and carefully mixed every 30 min. One percent Triton X-100 served as positive control, PBS served as negative control. H_2O was tested as vehicle control. To detect potential interferences of nanoparticles with the assay, the positive control was additionally spiked with nanoparticles. To determine the nanoparticle background, nanoparticles diluted in H_2O at the respective concentrations were used. After 3 h, samples were centrifuged at 800× g for 15 min. The supernatant was centrifuged again for 4 h at 18,000× g to sediment the nanoparticles. In order to determine the content of free hemoglobin, 100 μL supernatant was incubated with 100 μL Drabkin's reagent (Sigma-Aldrich) for 5 min in 96-well plates at 60 °C while heating. Drabkin's reagent lyses erythrocytes and converts hemoglobin and its derivatives to methemoglobin and then to cyanmethemoglobin. Absorption of the samples was measured at 590 nm on Microplate Reader Filter Max F5 (Molecular Devices, USA).

Plasma coagulation: Sodium citrate anticoagulated blood was centrifuged at 2500× g for 15 min to obtain platelet poor plasma (PPP). Nanoparticles were diluted in H_2O and incubated with PPP for 30 min at 37 °C (ratio 1:10). Thrombin time (TT), prothrombin time (PTT), and activated partial thromboplastin time (aPTT) were determined using coagulation kits obtained from DiaSys Diagnostic Systems GmbH (Holzheim, Germany) according to the manufacturer's instructions. The experiments were performed in the MC 4 Plus coagulometer (Merlin medical, Germany). Plasma samples with normal and abnormal coagulation times (obtained from DiaSys Diagnostic Systems GmbH, Germany) were used as negative and positive controls, respectively.

Complement activation: To analyze complement activation, an iC3b ELISA obtained from MicroVue (Quidel, USA) was performed. For this, sodium citrate anticoagulated blood was centrifuged for 10 min at 2500× g to obtain platelet-poor plasma (PPP). The PPP was mixed 1:1 with Veronal Buffer (Lonza, Switzerland). All nanoparticles were diluted to 1.2 and 0.3 mg/mL in H_2O and possessed an endotoxin level <0.1 EU/mL. Twenty-five microliters of the nanoparticles were added to 50 μL of the mixture of PPP and Veronal Buffer. H_2O served as negative control, cobra venom factor (CVF) and cremophor (both Quidel, USA) served as positive controls for complement activation. Additional samples with nanoparticles and CVF were prepared to analyze possible interferences by the nanoparticles (inhibition/enhance-ment controls, IEC). All samples were incubated at 37 °C for 30 min. Then, the samples were diluted in Specimen Diluent (CFV and IEC 1:25, other samples 1:100). The ELISA was performed according to the manufacturer's instructions. In brief, 100 μL iC3b Specimen Diluent (blank), standards, controls and samples were added to the assay plate and incubated for 30 min at RT. Then, the plate was washed five times with the washing buffer, followed by incubation with 50 μL iC3b conjugate for 30 min at RT. After that, the plate was again washed five times. Next, 50 μL 1× substrate solution was added and incubation continued for 30 min. Subsequently, 50 mL stop solution was added and the absorbance at 405 nm was analyzed with the Microplate Reader Filter Max F5 (Molecular Devices, USA). Thrombocyte activation: Platelet-rich plasma (PRP) was obtained from sodium citrate anticoagulated blood (centrifugation at 200× g for 30 min). PBS served as negative, H_2O as vehicle, and collagen (Collagen I, Rat Tail, Gibco, Life Technologies Corporation, USA) as positive control, respectively. The nanoparticles were diluted to 4 mg/mL and 1 mg/mL. Ninety microliter PRP was mixed with 10 μL sample into a prewarmed reaction tube and incubated for 15 min at 37 °C with continuous shaking. Subsequently, 50 μL of the samples were added to a FACS tube containing 100 μL PBS and the

number of non-aggregated platelets was determined by flow cytometry. Formation of neutrophil extracellular traps (NETosis): Polymorphonuclear leukocytes (PMN) were isolated from whole blood using ficoll density gradient centrifugation (Merck, Germany). PMN were adjusted to a density of 1×10^6 cells/mL and 225 µL was added to cell culture plates. Nanoparticles were diluted to 0.5, 1, 2, and 4 mg/mL. Phorbol-12-myristate-13-acetate (PMA) at 1 mM served as positive control. Cell medium and H_2O served as negative and vehicle controls. Twenty-five microliters of each sample was added to the cells and incubated for 4 h. Free PMN as well as agglomerates were analyzed in flow cytometry. In general, flow cytometry data were analyzed with Kaluza software 1.2 from Beckman Coulter (USA) and processed using Microsoft Excel (USA). All experiments were performed in triplicate, three times independently and the results were averaged.

In vivo Complement Activation in a Porcine Model

The protocol of Szebeni et al[39,40] was used to study the activation of the complement system in vivo. Briefly, domestic male Yorkshire pigs with a body weight of 20–25 kg were prepared for the treatment with different contrast agents by intubation with endotracheal tubes and anesthetization with isoflurane (2–3 vol%) in oxygen. All test substances were injected into the animals as a bolus via the left external jugular vein. The used contrast agent doses were 0.5 and 5.0 mg Fe/kg. Saline served as negative control and zymosan at a concentration of 0.1 mg/mL served as positive control. During the procedure, a CAP10 capnograph (Medlab, Germany) monitored the respiratory rate, as well as the end-expiratory CO_2 concentration, and the temperature was measured rectally. A pulse oximeter was fixed on the tail and the pulmonary artery pressure (PAP) was acquired through a Swan-Ganz catheter (AI-07124; Teleflex, Ireland) which was introduced into the pulmonary artery via the right jugular vein. The systemic arterial pressure (SAP) was recorded in the femoral artery. These hemodynamic changes were continuously monitored (sampling rate: 1 kHz) with an AD Instruments PowerLab System (Bella Vista, Australia) using LabChart Pro v6 software. In order to determine changes in platelets, white blood cells (WBC) and thromboxane B2 (TXB2) levels in plasma with an enzyme-linked immunosorbent assay (ELISA; Cayman Chemical Co., USA), blood samples were collected before and after the administration of the CA. Experiments were performed in duplicate for each contrast agent and each concentration; the results were averaged. The study was approved by the local ethics committee for animal experimentation (ÁTET, Hungary, Permit No. PE/EA/353-7/2020). The guidelines for animal welfare and animal testing of the Government of Hungary were followed in this study (Decree No 40/2013 [II. 14.]).

In vivo Magnetic Resonance Imaging in Rats

In vivo MRI studies were carried out with healthy male and female (50%/50%) Wistar rats (Janvier Labs, France) using a 3 T Philips Ingenia MRI system (Netherlands). A Philips 8-channel knee coil was used for the MRI acquisition and medetomidine/ketamine (0.5 mg/50 mg per kg body weight, respectively) was administered as intraperitoneal injection for animal anesthesia. The different formulations were administered via intravenous injection at a dose of 2.6 mg iron per kg body weight (mg Fe/kg), and animals were observed for signs of acute and delayed toxicity, afterwards. 2D multislice T_1-weighted turbo spin-echo (T_1w TSE), 2D multislice T_2-weighted turbo spin-echo with spectral attenuated inversion recovery for fat suppression (T_2w TSE SPAIR) and 3D 4-echo gradient echo T_2*-weighted (T_2*w FFE) imaging of the liver were performed before, as well as at 1, 3, 24, and 168 h after administration with the following parameters listed in Table 1. Imaging sequence parameters were chosen to minimize motion artifacts, which is why no respiratory gating was performed. Image analysis was made by manual region of interest (ROI) selection with the VivoQuant v. 1.22 software (USA). Hereby, the liver mean signal was normed to muscle mean signal on each scan to make the different scans comparable. The experiment was performed in triplicate for each formulation independently, and the results were averaged. The study was approved by the local ethics committee for animal experimentation (ÁTET, Hungary). The guidelines for animal welfare and animal testing of the Government of Hungary were followed in this study (Decree No 40/2013 [II. 14.]).

Table 1 Summary of MRI Acquisition Parameters for in vivo Imaging

Type of Scan	Repetition Time/Echo Time (ms/ms)	vField of View (mm³)	Resolution (mm³)	Gap Between Slices (mm)	Number of Animals
T₁w TSE	630.8/20	70 × 70 × 57	0.3125 × 0.3125 × 1.5	0.8	3
T₂w TSE SPAIR	2000/40	70 × 70 × 54	0.3125 × 0.3125 × 1.5	0.15	3
T₂*w FFE	11.173/6.638	70 × 70 × 64.5	0.49 × 0.49 × 1.5	–	3

Abbreviations: T_iw (i=1, 2 or 2*), T_i-weighted, TSE, turbo spin echo, SPAIR, spectral attenuated inversion recovery, FFE, fast field echo.

Statistical Analysis

Data are expressed as mean ± standard deviation, unless stated otherwise. Normality of the data was tested with the D'Agostino–Pearson omnibus K2 Test using Prism v. 9.4.1 (GraphPad Software, USA). After passed normality test, one-way analysis of variance (ANOVA) with the Bonferroni post-hoc test was performed in Prism in order to determine differences between the untreated control and the samples exposed to different contrast agent concentrations. Asterisks mark statistical significance: $*p < 0.05$, $**p < 0.01$, $***p < 0.001$, $****p < 0.0001$.

Results

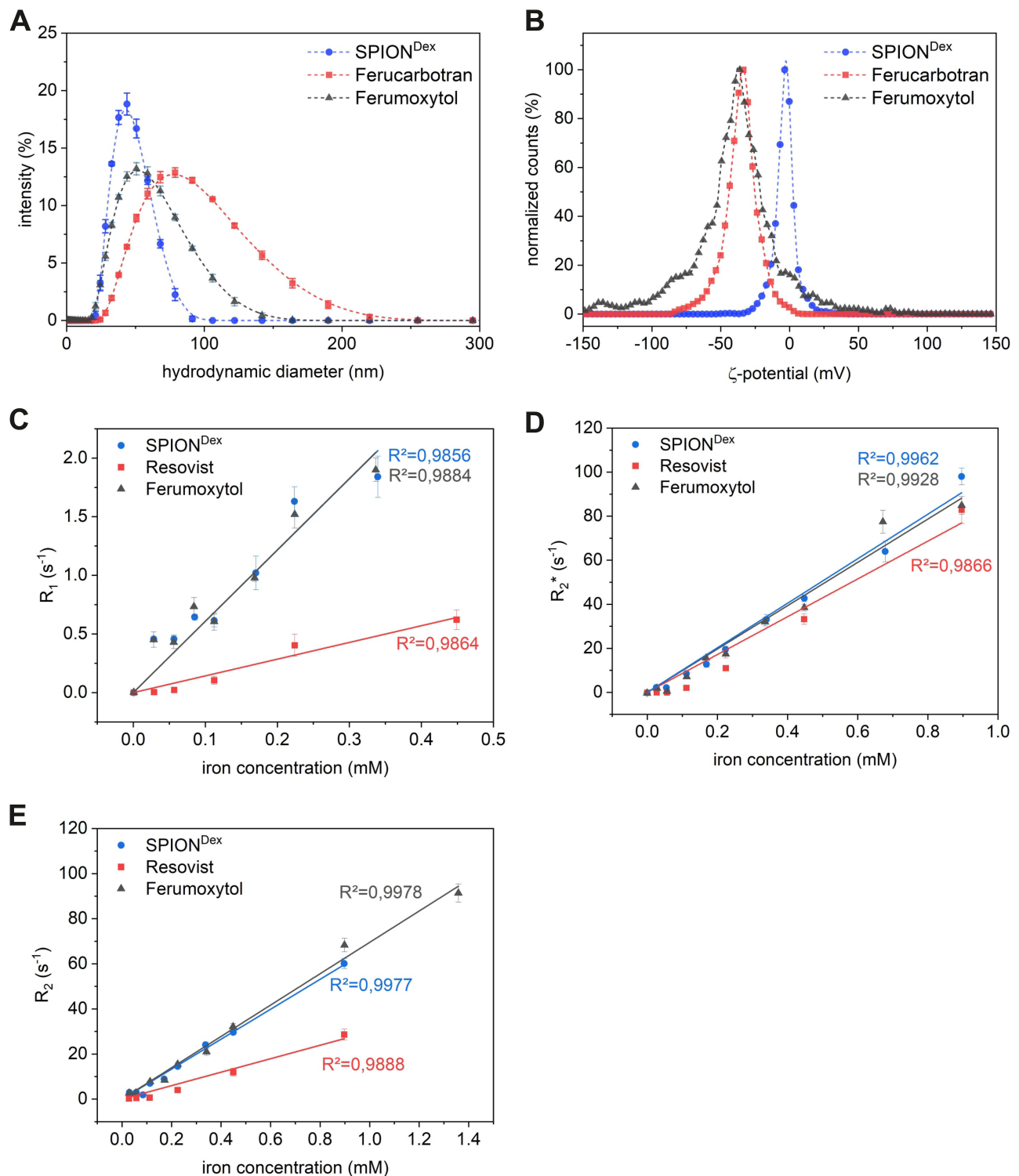## Physicochemical Comparison of the Contrast Agents

In order to better evaluate the differences in the toxicological profile of the different contrast agents and the outcome of the animal experiments, we first determined basic physicochemical parameters, which are summarized in Table 2. With a hydrodynamic size of 35 nm and a low polydispersity index (PDI) of 0.129, SPION^Dex were the smallest of the three compounds and had the narrowest size distribution (see Figures 1A, S1a and S1b). Ferumoxytol had a comparable size of 38 nm, whereas ferucarbotran particles were much larger (59 nm). Both ferumoxytol and ferucarbotran possessed a highly negative surface charge (−40 and −35 mV), in contrast to SPION^Dex that had only a slightly negative mean zeta potential of −4 mV (Figure 1B). TGA analysis showed comparable organic contents, ie, shell material, of approx 40–45 wt% (Figure S1c–e), but as expected, FTIR revealed the variation in the coating materials (Figure S1f). While all three spectra show typical peaks of carbohydrates, differences are visible in the finger-print region. SPION^Dex possessed typical vibrations of crosslinked dextran.[34] The spectrum of ferucarbotran differs in this respect in the C-O-C vibrational region, and in the appearance of another peak at 1591 cm⁻¹, representing the carboxyl functionalization of its dextran shell.[41] Typical peaks of the polyglucose sorbitol carboxymethyl ether coating were detectable in the spectrum of ferumoxytol.[42] For 3T MRI, R_1, R_2 and R_2* relaxation rates were measured using different MRI protocols to determine

Table 2 Summary and Comparison of the Contrast Agent Formulations' Different Physicochemical Properties

Property	SPION^Dex	Ferucarbotran	Ferumoxytol
Hydrodynamic size (nm)	35 ± 0.1	59 ± 0.1	38 ± 0.2
Polydispersity index (a.u.)	0.129 ± 0.005	0.180 ± 0.013	0.210 ± 0.001
ζ-Potential (mV) at pH 7.4	−4 ± 0.3	−35 ± 0.4	−40 ± 0.5
Magnetic volume susceptibility normalized to iron concentration (mL/mg)	$9.0 \times 10^{-4} \pm 4 \times 10^{-6}$	$7.7 \times 10^{-3} \pm 9 \times 10^{-7}$	$1.5 \times 10^{-3} \pm 3 \times 10^{-7}$
r_1 (s⁻¹mM⁻¹)	6 ± 0.4	1.4 ± 0.1	6 ± 0.4
r_2 (s⁻¹mM⁻¹)	66 ± 1.6	30 ± 2.0	67 ± 1.7
r_2* (s⁻¹mM⁻¹)	101 ± 3.0	86 ± 5.8	98 ± 4.0

Note: Mean ± SD of n=3 experiments are shown.
Abbreviations: r_i, relaxivity of T_i-weighted sequences (i= 1, 2 or 2*), SPION^Dex, dextran-coated superparamagnetic iron oxide nanoparticles, SD, standard deviation.

Figure 1 Comparison of physicochemical properties of the particles. (**A**) Intensity-weighted hydrodynamic size distribution. (**B**) ζ-potential distribution at pH 7.4. 3 T MRI derived T_1 (**C**), T_2 (**D**) and T_2^* (**E**) relaxation rates as a function of iron concentration. The relaxivity r is derived from the slope of the corresponding linear fit.
Notes: For (**A** and **B**): representative result of one experiment. For (**C–E**): mean ± SD of n=3 experiments are shown.
Abbreviations: R_i, relaxation rate of T_1-weighted sequences (i= 1, 2 or 2*), SPION^{Dex}, dextran-coated superparamagnetic iron oxide nanoparticles, SD, standard deviation.

the contrast agent relaxivity values r_1, r_2 and r_2^* as a measure of in vitro MRI contrast efficiency (see Figure 1C–E). Ferumoxytol and SPION^{Dex} showed similar relaxivity values, but ferucarbotran was less potent under the tested conditions for all three sequences (see Table 2).

Nanoparticulate Contrast Agent-Induced Cytotoxicity

In this study, contrast agent cytotoxicity was investigated using the non-adherent human T cell leukemia cell line Jurkat. These cells were treated with iron concentrations up to 400 µg/mL for 24 and 48 h, followed by flow-cytometric examination of cell death markers. Initially, we examined phosphatidylserine exposure by AxV staining, and plasma membrane integrity by PI staining (Figure 2A) in order to distinguish between viable (AxV-PI-), apoptotic (AxV+PI-) and necrotic (PI+) cells. After 24 h incubation with SPION^{Dex} or ferumoxytol, a very weak, dose-dependent impact on cell viability was observed, but it was not statistically significant. In contrast, ferucarbotran significantly reduced cell viability already at 50 µg/mL. The same trend was also evident when measuring the loss of mitochondrial membrane potential (Figure S2a). However, no changes in cell cycle, such as cell cycle block or DNA degradation due to activation of DNAses during apoptosis, were observable upon contrast agent treatment (Figure S2b). Ferucarbotran also showed a significant increase in the side scatter intensity (Figure 2B), indicative of cellular uptake of nanoparticles.[43] In contrast, side scatter intensity was not increased for SPION^{Dex} and ferumoxytol. To obtain information on the amount of oxygen/nitrogen radicals and cellular glutathione status (oxidized/reduced) after nanoparticle administration, combined staining with 2',7'-dichlorofluorescin (DCFH) and monobromobimane (MBB) were performed and evaluated using flow cytometry. DCFH staining after 24 h of incubation with the nanoparticles revealed a very weak, yet not significant fluorescence signal increase at the highest tested concentration (400 µg/mL) for ferucarbotran and ferumoxytol (Figure 2C). No significant increase in DCFH signal was observed in cells exposed to SPION^{Dex}, even at 400 µg/mL. In addition, the MBB fluorescence was also not significantly altered after 24 h, (Figure S2c) confirming the results of the DCFH measurements.

Particle Hemocompatibility

To prevent the clogging of blood vessels by agglomerating nanomaterials, their colloidal stability in human blood must be confirmed. To test this, human whole blood was anticoagulated with different substances (lithium heparin, EDTA, sodium citrate) to exclude effects of the anticoagulant itself. Figure S3 shows representative example results from one donor at an iron concentration of 250 µg/mL. Across the all three donors, no particle agglomerates were detectable under the microscope for any of the three nanoparticle formulations. Since the resolution of the used light microscope is about 200 nm, it can be assumed that no agglomerates larger than this limit occur under the tested conditions. In addition, none of the formulations produced hemolysis (Figure S2d). Another important factor is blood coagulation, a complex multi-component process with three main activation pathways: intrinsic, extrinsic and common. To analyze whether coagulation is induced by the different nanoparticles, platelet-poor plasma was preincubated with the respective nanomaterials for 30 minutes at 37 °C. Figure 2D shows the results of the aPPT test, a measure for the intrinsic blood coagulation pathway. While SPION^{Dex} had no effect on aPPT even at the highest concentration, ferucarbotran massively inhibited the intrinsic pathway and its effect at the highest tested concentration exceeded even the positive control. Ferumoxytol at 400 µg/mL slightly but not significantly increased the aPPT. In addition, the extrinsic pathway determined by the prothrombin time (Figure S2e) was not influenced by the contrast agents, while the common pathway, reflected by the thrombin time values, was significantly inhibited by ferucarbotran at a concentration of 400 µg/mL (Figure S2f). The Interaction of platelets with nanoparticles was investigated using platelet-rich plasma (PRP). After incubation with CA, the aggregation of platelets was determined by flow cytometry. Compared to the negative control, no significant increase in aggregated platelets was determined (Figure 2E). After induction of platelet aggregation in the CA-containing PRP by collagen (10 µg/mL), in the presence of ferucarbotran, lower numbers of platelet aggregates were detected, whereas SPION^{Dex} and ferumoxytol did not interfere with collagen-induced platelet aggregation (data not shown). Beyond these well-known pathways, there is another possibility how SPIONs potentially can induce blood clotting, namely by the formation of neutrophil extracellular traps (NETosis). In order to test this, isolated polymorphonuclear leukocytes (PMN) were incubated with the respective contrast agents for 3 h and the number of not agglomerated PMN was subsequently determined by flow cytometry. The positive control phorbol-12-myristate-13-acetate (PMA) induced NETosis, leading to a reduced amount of free PMN (Figure 2F). In contrast, none of the three formulations affected the PMN count as the positive control but ferucarbotran showed a mild significant reduction at the highest tested concentration.
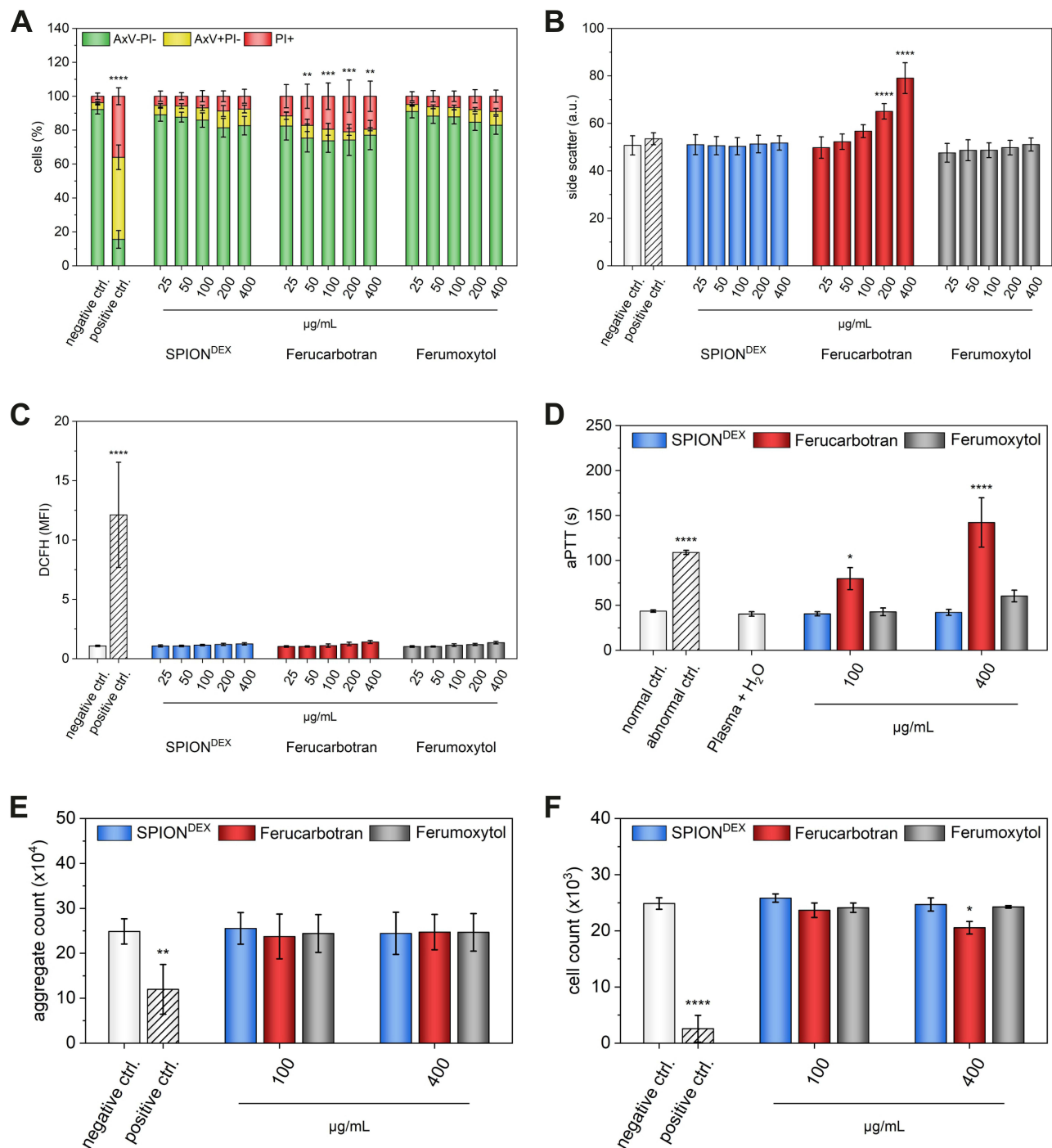
Figure 2 Cytotoxicity of nanoparticles. (**A**) Viability of Jurkat cells after treatment with nanoparticles for 24 h determined by AxV-PI staining. (**B**) Cellular nanoparticle uptake determined by FACS side scatter intensity. (**C**) Reactive oxygen species formation in cells measured by DCFH fluorescence. (**D**) Effect of contrast agents on intrinsic blood coagulation pathway. (**E**) Activation of thrombocytes. (**F**) Formation of neutrophil extracellular traps.
Notes: Asterisks mark the significance levels after passed normality test (*p < 0.05, **p < 0.01, ***p < 0.001, ****p < 0.0001). For (**A–C**) mean ± SD of n=5 experiments are shown. For (**D–F**) mean ± SD of n=3 experiments are shown.
Abbreviations: SPION^{Dex}, dextran-coated superparamagnetic iron oxide nanoparticles, a.u., arbitrary units, DCFH, 2'-7'dichlorofluorescin, aPTT, activated partial thromboplastin time, SD, standard deviation.

Contrast Agents Show Strong Differences in Complement Activation

The complement system is an essential part of the innate immunity, contributing to a non-specific host defense. It consists of a set of plasma proteins that activate each other by cleavage. The complement cascade can be activated by immune complexes (classical pathway), in antibody-independent manner (alternative pathway), or by mannose-binding lectin

(lectin pathway). Here, the formation of the cleavage product iC3b that occurs in all three pathways was analyzed using ELISA, showing a strong signal for the control substance cobra venom factor (CVF), but also for Cremophor-EL, which is used in pharmaceutical industry as an excipient to dissolve hydrophobic drugs, eg, Taxol, and is known to form nanosized micelles causing complement activation.[44] Ferumoxytol strongly induced iC3b formation and the extent of this increase exceeded even the effect of the Cremophor-EL mix (Figure 3A). In samples treated with ferucarbotran or SPION^{Dex} no significant iC3b increase was detected. The data also demonstrated large variability in the responses among different donors. The next step was to evaluate the complement activation-related pseudoallergy (CARPA) response in a porcine model.[33,45] Prior to the injection of the respective contrast agent at 5 mg iron per kg body weight, saline was injected as negative control. Each experiment was then finished by the injection of zymosan as positive control. The comparison of hemodynamic changes induced by the three nanoparticle formulations demonstrated significant differences in animal responses to injections. Administration of SPION^{Dex} (Figure 3B) showed only a very mild increase in PAP (approx 15%) and no changes in heart rate (HR) or systemic arterial blood pressure (SAP) were observed. In contrast, ferucarbotran (Figure 3C) evoked a massive increase in PAP. Ferumoxytol administration (Figure 3D) did not only induce a strong PAP increase but also led to anaphylaxis that required subsequent cardiopulmonary resuscitation (CPR) involving heart massage and intra-cardiac epinephrine injection, resulting in an increase in HR and SAP. Animals treated with particles at a dose reduced to only one-tenth of the original particle dose (ie, to 0.5 mg iron per kg body weight) showed the same behavior (Figure S4a–c). Besides the significant increase in maximal PAP for all ferucarbotran- and ferumoxytol-treated animals (Figure 3E), an increase in the biomarker TXB2 (Figure 3F), as well as a decrease in white blood cells (Figure S4d) and platelet counts (Figure S4e) was observable, too. Beyond that, rashes and flushes appeared in some of these animals shortly after the injection (Figure 3G).

Kinetics of Liver Imaging in Rats

The comparison of liver imaging performance and kinetics was done in rats. Accordingly, T_1- (Figure S5a), T_2- (Figure S5b) and T_2*-weighted MRI scans (Figure 4A) of each animal were performed before and at 1 h, 3 h, 24 h and 168 h after particle injection at a dose of 2.6 mg Fe/kg. All three MRI sequences showed strong iron oxide-induced signal attenuation as early as 1 h after contrast agent administration, regardless of the contrast agent used. However, the time course of clearance strongly differed for the different particle types. While the signal attenuation in T_2*-weighted images induced by SPION^{Dex} became significantly smaller beyond 24 hours, it remained strongly visible even after one-week post administration in animals treated with ferucarbotran or ferumoxytol. Since the interpretation of MRI images is often highly subjective in nature, several areas were manually selected on the liver parenchyma during each scan to compare the normalized mean signal intensity of these areas with the pre-contrast scans. Care was taken to avoid portal veins, hepatic veins, or imaging artifacts when selecting areas. The results shown in Figure 4B–D confirmed that while all three candidates produce a strong negative contrast already after 1 h, especially in the T_2- and T_2*-weighted MRI images relevant for iron oxide-based contrast agents, a strong recovery of the signal intensity to the pre-administration status within 1 week was only observable for SPION^{Dex}.

Discussion

Iron oxide-based contrast agents represent a viable alternative to GBCA, at least in some areas of applications. The aim of the current study was to evaluate the risk-to-benefit profile of different formulations and the potential advantages of SPION^{Dex} over ferucarbotran and ferumoxytol, which previously showed adverse effects in humans. In order to better understand the differences observed among the contrast agents, their basic physicochemical properties were compared. While the coating of SPION^{Dex} consists of cross-linked dextran, the FTIR spectrum of ferucarbotran showed a less smeared C-O-C vibrational region, indicating the absence of cross-linking, and an appearance of another peak at 1591 cm^{-1}, representing the carboxyl functionalization of its dextran shell, that contributes to its high surface charge.[41] Also in ferumoxytol, carboxyl groups are responsible for the high negative surface charge.[42] Despite strong differences in surface charge, all three nanoparticle formulations were characterized with a good colloidal stability in aqueous media and blood, which can be attributed to good electrosteric or steric stabilization due to their respective carbohydrate coating.[46] Despite its larger hydrodynamic size as compared with the other two formulations, ferucarbotran has lower relaxivity values in the direct comparison at the given parameters. However, relaxivity values are highly
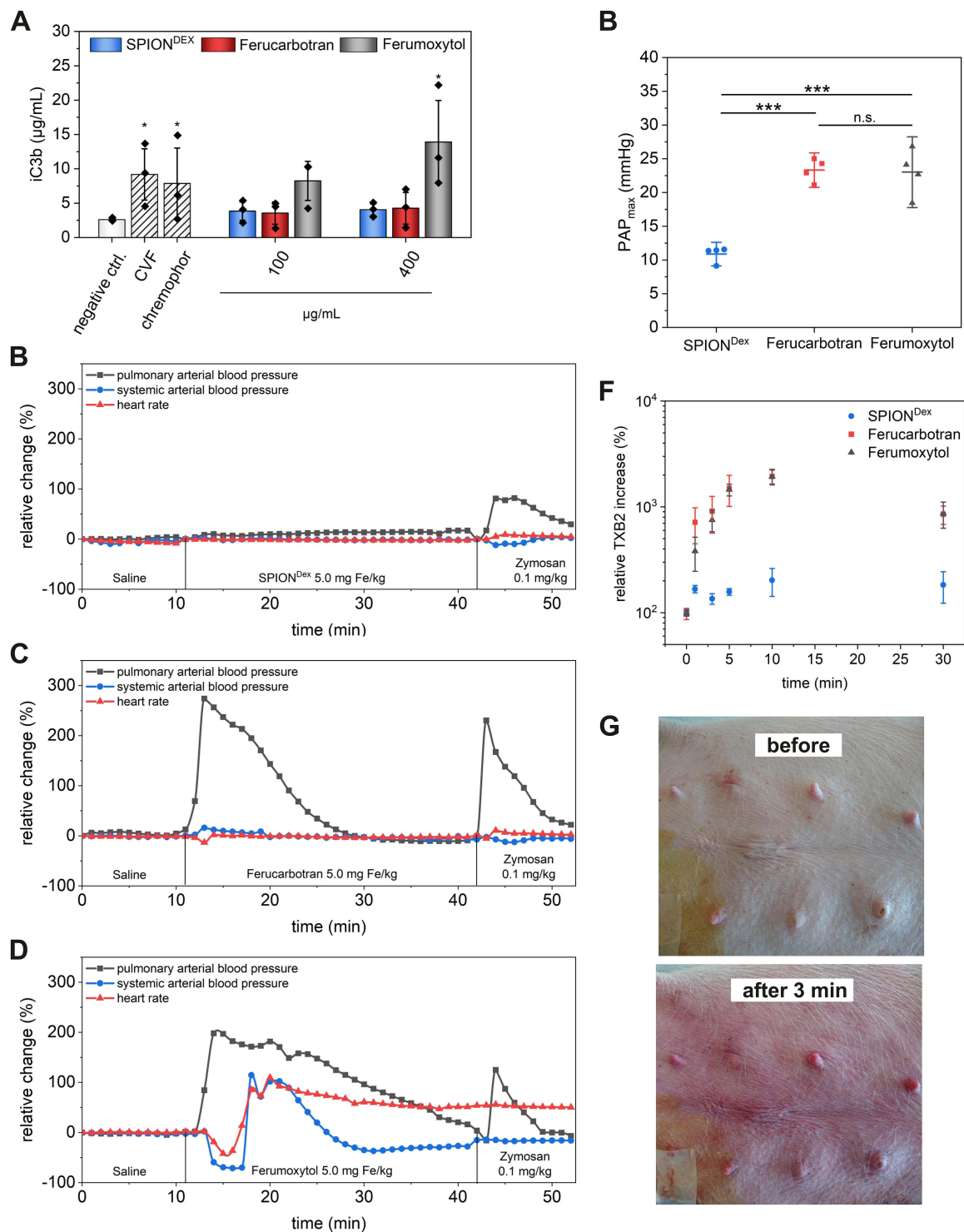
Figure 3 Contrast agent-induced complement activation. (**A**) Determination of the iC3b split product, in human-derived platelet-poor plasma (n=3). Relative hemodynamic changes as indication of in vivo complement activation in a porcine model after administration of SPION^{Dex} (**B**), ferucarbotran (**C**), and ferumoxytol (**D**) at an iron concentration of 5 mg/kg. The latter resulted in anaphylaxis and requiring subsequent cardiopulmonary resuscitation. (**E**) Comparisons of maximum pulmonary artery pressure after contrast agent application (data for both doses, 0.5 and 5.0 mg Fe/kg, are pooled). (**F**) Normalized thromboxane B2 levels in pigs acquired from blood samples collected during application. (**G**) Example image of flushes appearing in the abdominal region after ferumoxytol application.

Notes: Asterisks mark the significance levels after passed normality test (***p < 0.01, ***p < 0.001, ****p < 0.0001). For (**A**): mean ± SD of n=3 experiments are shown. For (**B–D**): representative result of one experiment are shown. For (**E** and **F**): mean ± SD of n=4 experiments are shown (data for both doses, 0.5 and 5.0 mg Fe/kg, are pooled).

Abbreviations: SPION^{Dex}, dextran-coated superparamagnetic iron oxide nanoparticles, iC3b, protein fragment that is part of the complement system, CVF, cobra venom factor, PAP$_{max}$, maximum pulmonary artery pressure, TXB2, thromboxane B2, SD, standard deviation.
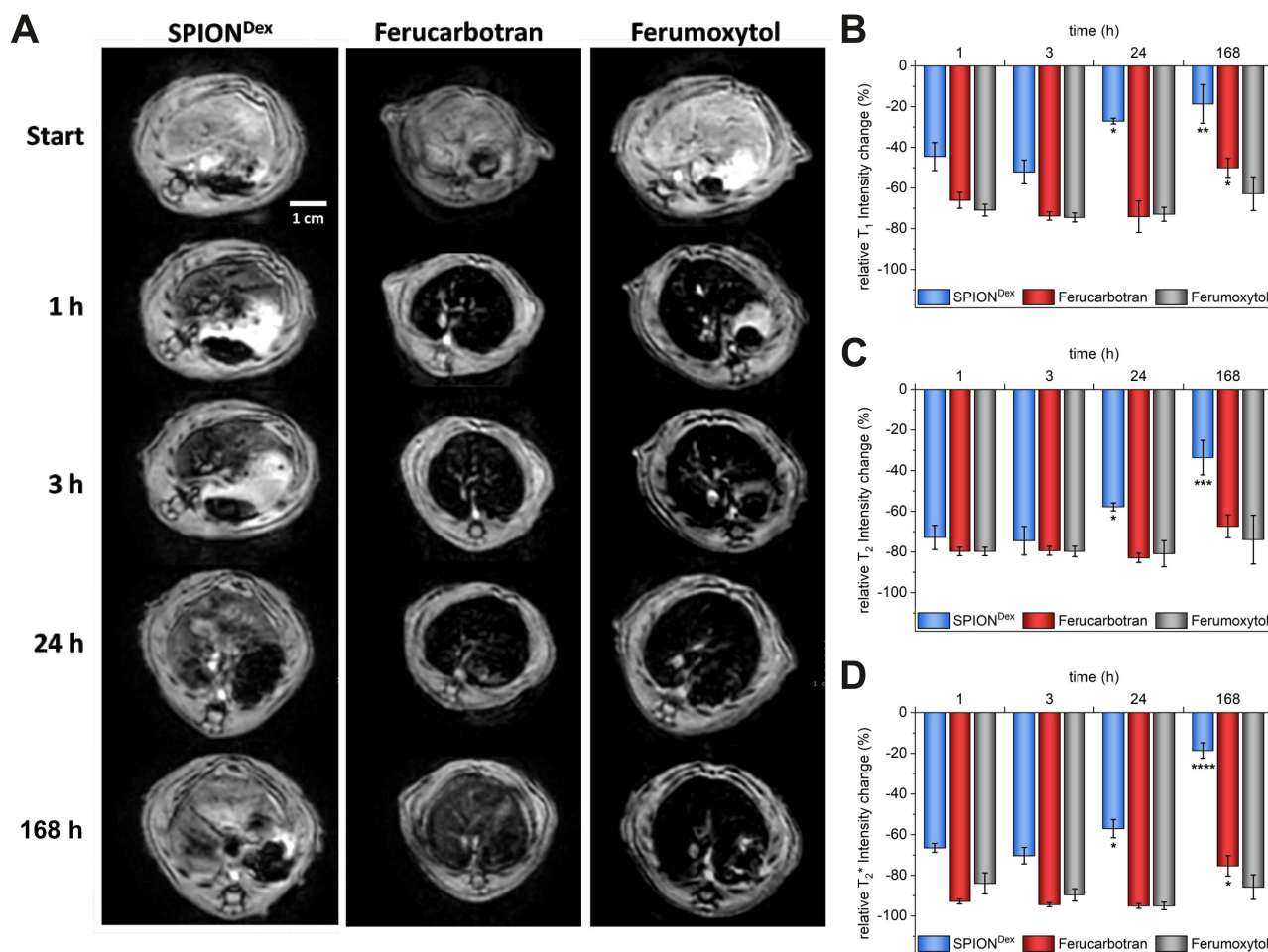
Figure 4 MRI experiments in rats. (**A**) Exemplary transversal T_2*-weighted MRI of a rat's liver before and at specific time points after administration of contrast agents at an iron dose of 2.6 mg Fe /kg. Qualitative evaluation of liver uptake and elimination of contrast agents from the liver based on T_1-weighted (**B**), T_2-weighted (**C**), and T_2*-weighted (**D**) scans (n=3).
Notes: Asterisks mark the significance levels after passed normality test (*p < 0.05, **p < 0.01, ***p < 0.001, ****p < 0.0001). Mean ± SD of n=3 experiments are shown.
Abbreviations: SPION^{Dex}, dextran-coated superparamagnetic iron oxide nanoparticles, SD, standard deviation.

dependent on the used MRI parameters, as an r_2 value of 151 mM^{-1}s^{-1} was previously reported for ferucarbotran.[29] Typical r_1 and r_2 values for GBCAs are both in the range of approx 5 s^{-1}mM^{-1}.[47] Ferumoxytol and SPION^{Dex} therefore have 13 times higher r_2/r_1 and 20 times higher r_2*/r_1 ratio while the respective ratios are 6 and 17 times higher for ferucarbotran. This explains the ability of iron-oxide-based nanoparticles to create negative contrast at much lower concentrations as required for GBCAs to create positive contrast. Interestingly, the differences in relaxivities among the investigated iron oxide-based contrast agent do not translate directly into the in vivo imaging performance in rats. A simple explanation may be that in the in vitro experiments water is used instead of, eg, serum, which can have an effect on the relaxivity.[48] Further, the biodistribution behavior of the contrast agents may differ. SPION^{Dex} may have a longer blood half-life, so that their tissue/blood pool level differs from that of ferumoxytol or ferucarbotran. Interestingly, the MRI signal recovery in the rats' livers implies that SPION^{Dex} are metabolized or excreted from the liver more rapidly than other formulations, whereas ferucarbotran and ferumoxytol remain much longer in the liver and thus presumably in the patient's body. As a result, SPION^{Dex} administration could enable the repeated imaging for disease monitoring.

For the purpose of serial imaging, however, the contrast agent must be free of the risk of hypersensitivity reactions upon repeated administration, which may affect cellular, hemostasis-related and immune processes. Among the tested contrast agents, only ferucarbotran showed a significant cytotoxic effect in Jurkat cells, which correlated with an increased side scatter intensity, a measure of cellular particle uptake.[43] In contrast, side scatter intensity was not affected

by treatment with SPION^Dex or ferumoxytol, suggesting only a limited – if any – internalization of these particles. In previous studies, SPION^Dex showed no cytotoxic effects on human endothelial cells, macrophages and THP-1 cells.[34] At the highest tested concentrations of ferumoxytol and ferucarbotran, DCFH and MBB measurement indicated a small, but not statistically significant amount of reactive oxygen species (ROS). As a result, no upregulation of the thiol levels was observed in the treated cells, which may indicate that the induced oxidative stress was not strong enough to disturb redox-homeostasis of the cells.

Interference with blood coagulation pathways is one of the potential pitfalls in the clinical translation of nanoparticles.[49] Our results demonstrated that ferucarbotran strongly inhibited the intrinsic pathway of coagulation cascade, to the degree that exceeded the abnormal plasma control at the highest particle concentration. Ferucarbotran-induced inhibition of the common pathway was weaker, but still present. Incubation with ferumoxytol also caused an inhibition of the intrinsic pathway, but its effect was far less pronounced and SPION^Dex did not influence any of the coagulation pathways under the given conditions. Neither the extrinsic pathway nor platelet activation was affected by any of the contrast agents.

The most important aspect in clinical translation of parenterals is immunogenicity, especially when those agents are used for diagnostic purposes. In treatment and prevention, eg vaccination, a specific immune response is desired, but in diagnostics such a response usually leads to adverse effects, therefore stringent investigations of particle immunogenicity are required.[50] Upon intravascular injection of particles, the first line of immune defense they encounter are neutrophils, which either remove them by phagocytosis, inactivate them, or immobilize them by formation of NETs. As previously reported, nanoparticles can induce NET formation depending on their physicochemical properties such as size, coating and agglomeration status,[51] but our data indicated that only ferucarbotran at 400 μg/mL led to a moderate increase in NET formation. The next line in the immune defense, the complement system, is an essential part of the innate immunity, contributing to a non-specific host defense and can be activated by immune complexes (classical pathway), by an antibody-independent manner (alternative pathway), or by mannose-binding lectin (lectin pathway). The complement system can support recognition and clearance of pathogens and/or particles by their opsonization (C3b), but the uncontrolled production of proinflammatory anaphylatoxins (C3a, C4a, C5a) upon complement activation can stimulate the release of additional inflammatory mediators (eg histamine) by immune cells. This potentially life-threatening cascade of inflammatory events can be observed upon particle injection in vivo, in a model of CARPA.[45] Several nanoparticulate drugs in clinical use (eg Doxil, Taxol) have been reported to cause hypersensitivity reactions similar to CARPA in patients.[52] In vitro complement activation by nanoparticles in plasma have been reported to correlate with in vivo complement-mediated reactions.[53,54] To gain understanding of the contrast agents' potential to activate the complement system, we first incubated them in vitro with human sera. As expected, there was a large variability in the responses among donors, because complement is part of the innate immune system. However, a very clear tendency towards activation of the complement system was observed in ferumoxytol-treated samples, partially exceeding the effects of the positive controls. Subsequently, we tested whether the contrast agents cause CARPA reactions in an in vivo porcine model.[39] Symptoms of CARPA include hemodynamic and cardiopulmonary changes, with the increase in pulmonary arterial pressure (PAP) in pigs being the most common.[45] In addition, hematologic changes such as leukopenia or leukocytosis, thrombocytopenia, skin reactions and elevated thromboxane B2 (TXB2), as well as C-reactive protein levels are also important biomarkers of CARPA.[45] The results demonstrated that both ferumoxytol and ferucarbotran induced strong CARPA reactions in pigs even at low doses. Of note, the occurrence of CARPA in response to ferumoxytol was proportional to the increase of complement split product induced by this formulation in vitro. In contrast, the CARPA-genic activity of ferucarbotran did not correlate with its in vitro effects. This may be due to the fact that multiple pathways are activated during CARPA in vivo, including anaphylatoxin induction of mast cells and macrophages, as well as subsequent release of vasoactive and inflammatory mediators, in addition to C-activation. Nevertheless, the CARPA reactions observed in ferumoxytol-treated animals were more severe and the resulting anaphylaxis required subsequent cardiopulmonary reanimation. This is a very important finding as CARPA reactions are very likely responsible for the occurrence of adverse/hypersensitivity effects in patients administered SPION-based contrast agents and may affect risk-to-benefit profile of these formulations.[29,30,54,55] Irrespective of the applied dose, SPION^Dex did not evoke any CARPA reactions. The reason for this could be related to the design and morphology of

these nanoparticles, in which they differ from both ferucarbotran and ferumoxytol. Due to the crosslinking of dextran coating in SPION^{Dex}, the sugar structure of the coating is altered. In contrast to its native form, such a crosslinked dextran structure actually prevents complement activation in mice, as shown by Wang et al.[56] In addition, according to Chao et al, an exposed iron oxide surface provides an anionic charge pattern recognizable by scavenging receptors.[57,58] It can thus be assumed that crosslinking of dextran adsorbed on the surface of the particles leads to a denser surface coverage and, therefore, to a better shielding against these receptors.

Conclusion

In all toxicological studies, the SPION^{Dex} performed equally or significantly better than the two reference products. As a result, upon their clinical translation, SPION^{Dex} may provide a safer diagnostic agent with less adverse side effects. SPION^{Dex} are already upscaled and the cGMP compliant production processes required for translation are well advanced. Before they can be ultimately applied in their first-in-human trials, they have to pass mandatory regulatory safety tests performed by certified laboratories.

Acknowledgments

Disclosure

Dr Domokos Máthé reports being a stakeholder and the CEO from CROmed Ltd, outside the submitted work. Dr Kang H Zheng reports grants from EU - Nanoathero, during the conduct of the study. Prof. Dr Erik Stroes reports personal fees from Amgen, personal fees from Sanofi, personal fees from Astra-Zeneca, personal fees from Novo-Nordisk, grants from Ionis, personal fees from Daiichi-Sankyo, outside the submitted work. The authors report no other conflicts of interest in this work.

References

1. Hunt CH, Hartman RP, Hesley GK. Frequency and severity of adverse effects of iodinated and gadolinium contrast materials: retrospective review of 456,930 doses. *AJR Am J Roentgenol.* 2009;193(4):1124–1127. doi:10.2214/AJR.09.2520

2. Prince MR, Zhang H, Zou Z, Staron RB, Brill PW. Incidence of immediate gadolinium contrast media reactions. *AJR Am J Roentgenol.* 2011;196 (2):W138–W143. doi:10.2214/AJR.10.4885

3. Kanda T, Ishii K, Kawaguchi H, Kitajima K, Takenaka D. High signal intensity in the dentate nucleus and globus pallidus on unenhanced T1-weighted MR images: relationship with increasing cumulative dose of a gadolinium-based contrast material. *Radiology.* 2014;270(3):834–841. doi:10.1148/radiol.13131669

4. Radbruch A, Weberling LD, Kieslich PJ, et al. Gadolinium retention in the dentate nucleus and globus pallidus is dependent on the class of contrast agent. *Radiology.* 2015;275(3):783–791. doi:10.1148/radiol.2015150337

5. Roberts DR, Holden KR. Progressive increase of T1 signal intensity in the dentate nucleus and globus pallidus on unenhanced T1-weighted MR images in the pediatric brain exposed to multiple doses of gadolinium contrast. *Brain Dev.* 2016;38(3):331–336. doi:10.1016/j. braindev.2015.08.009

6. Miller JH, Hu HH, Pokorney A, Cornejo P, Towbin R. MRI brain signal intensity changes of a child during the course of 35 gadolinium contrast examinations. *Pediatrics.* 2015;136(6):e1637–1640. doi:10.1542/peds.2015-2222

7. Gulani V, Calamante F, Shellock FG, Kanal E, Reeder SB. Gadolinium deposition in the brain: summary of evidence and recommendations. *Lancet Neurol.* 2017;16(7):564–570. doi:10.1016/S1474-4422(17)30158-8

8. U.S. Food and Drug Administration. FDA Drug Safety Communication: FDA warns that gadolinium-based contrast agents (GBCAs) are retained in the body; requires new class warnings; 2018.

9. European Medicines Agency - Pharmacovigilance Risk Assessment Committee. PRAC concludes assessment of gadolinium agents used in body scans and recommends regulatory actions, including suspension for some marketing authorisations. EMA/157486/2017; 2017.

10. Senpan A, Caruthers SD, Rhee I, et al. Conquering the dark side: colloidal iron oxide nanoparticles. *ACS Nano.* 2009;3(12):3917–3926. doi:10.1021/nn900819y

11. Richards JM, Shaw CA, Lang NN, et al. In vivo mononuclear cell tracking using superparamagnetic particles of iron oxide: feasibility and safety in humans. *Circ Cardiovasc Imaging.* 2012;5(4):509–517. doi:10.1161/CIRCIMAGING.112.972596

12. Liu W, Frank JA. Detection and quantification of magnetically labeled cells by cellular MRI. *Eur J Radiol.* 2009;70(2):258–264. doi:10.1016/j. ejrad.2008.09.021

13. Diwoky C, Liebmann D, Neumayer B, et al. Positive contrast of SPIO-labeled cells by off-resonant reconstruction of 3D radial half-echo bSSFP. *NMR Biomed.* 2015;28(1):79–88. doi:10.1002/nbm.3229

14. Israel LL, Galstyan A, Holler E, Ljubimova JY. Magnetic iron oxide nanoparticles for imaging, targeting and treatment of primary and metastatic tumors of the brain. *J Control Release.* 2020;320:45–62. doi:10.1016/j.jconrel.2020.01.009

15. Fülöp T, Nemes R, Mészáros T, et al. Complement activation in vitro and reactogenicity of low-molecular weight dextran-coated SPIONs in the pig CARPA model: correlation with physicochemical features and clinical information. *J Control Release*. 2018;270:268–274. doi:10.1016/j.jconrel.2017.11.043

16. Abdollah MRA, Carter TJ, Jones C, et al. Fucoidan prolongs the circulation time of dextran-coated iron oxide nanoparticles. *ACS Nano*. 2018;12 (2):1156–1169. doi:10.1021/acsnano.7b06734

17. Antonelli A, Pacifico S, Sfara C, Tamma M, Magnani M. Ferucarbotran-loaded red blood cells as long circulating MRI contrast agents: first in vivo results in mice. *Nanomedicine*. 2018;13(7):675–687. doi:10.2217/nnm-2017-0339

18. Taruno K, Kurita T, Kuwahata A, et al. Multicenter clinical trial on sentinel lymph node biopsy using superparamagnetic iron oxide nanoparticles and a novel handheld magnetic probe. *J Surg Oncol*. 2019;120(8):1391–1396. doi:10.1002/jso.25747

19. Cohen J, Khudanyan A, Lu J, et al. A multicenter study evaluating the effectiveness and safety of single-dose low molecular weight iron dextran vs single-dose ferumoxytol for the treatment of iron deficiency. *Am J Hematol*. 2020;95(12):1572–1577. doi:10.1002/ajh.25995

20. Karki NR, Auerbach M. Single total dose infusion of ferumoxytol (1020 mg in 30 minutes) is an improved method of administration of intravenous iron. *Am J Hematol*. 2019;94(9):E229–E231. doi:10.1002/ajh.25548

21. Turkbey B, Czarniecki M, Shih JH, et al. Ferumoxytol-enhanced MR lymphography for detection of metastatic lymph nodes in genitourinary malignancies: a prospective study. *AJR Am J Roentgenol*. 2020;214(1):105–113. doi:10.2214/AJR.19.21264

22. Carney BW, Gholami S, Fananapazir G, et al. Utility of combined gadoxetic acid and ferumoxytol-enhanced liver MRI for preoperative detection of colorectal cancer liver metastases: a pilot study. *Acta Radiol*. 2022:2841851221136499. doi:10.1177/02841851221136499

23. Daldrup-Link HE, Theruvath AJ, Rashidi A, et al. How to stop using gadolinium chelates for magnetic resonance imaging: clinical-translational experiences with ferumoxytol. *Pediatr Radiol*. 2022;52(2):354–366. doi:10.1007/s00247-021-05098-5

24. Siedek F, Muehe AM, Theruvath AJ, et al. Comparison of ferumoxytol- and gadolinium chelate-enhanced MRI for assessment of sarcomas in children and adolescents. *Eur Radiol*. 2020;30(3):1790–1803. doi:10.1007/s00330-019-06569-y

25. Hamilton BE, Barajas R, Nesbit GM, et al. Ferumoxytol-enhanced MRI is not inferior to gadolinium-enhanced MRI in detecting intracranial metastatic disease and metastasis size. *AJR Am J Roentgenol*. 2020;215(6):1436–1442. doi:10.2214/AJR.19.22187

26. Barajas RF, Hamilton BE, Schwartz D, et al. Combined iron oxide nanoparticle ferumoxytol and gadolinium contrast enhanced MRI define glioblastoma pseudoprogression. *Neuro Oncol*. 2019;21(4):517–526. doi:10.1093/neuonc/noy160

27. Queler SC, Tan ET, Geannette C, Prince M, Sneag DB. Ferumoxytol-enhanced vascular suppression in magnetic resonance neurography. *Skeletal Radiol*. 2021;50(11):2255–2266. doi:10.1007/s00256-021-03804-w

28. Aghighi M, Pisani L, Theruvath AJ, et al. Ferumoxytol is not retained in kidney allografts in patients undergoing acute rejection. *Mol Imaging Biol*. 2018;20(1):139–149. doi:10.1007/s11307-017-1084-8

29. Wang Y-XJ. Superparamagnetic iron oxide based MRI contrast agents: current status of clinical application. *Quant Imaging Med Surg*. 2011;1 (1):35–40. doi:10.3978/j.issn.2223-4292.2011.08.03

30. Hsiao YP, Huang CH, Lin YC, Jan TR. Systemic exposure to a single dose of ferucarbotran aggravates neuroinflammation in a murine model of experimental autoimmune encephalomyelitis. *Int J Nanomedicine*. 2019;14:1229–1240. doi:10.2147/IJN.S189327

31. Nguyen KL, Yoshida T, Kathuria-Prakash N, et al. Multicenter safety and practice for off-label diagnostic use of ferumoxytol in MRI. *Radiology*. 2019;293(3):554–564. doi:10.1148/radiol.2019190477

32. U.S. Food and Drug Administration. FDA strengthens warnings and changes prescribing instructions to decrease the risk of serious allergic reactions with anemia drug Feraheme (ferumoxytol); 2015.

33. Unterweger H, Janko C, Schwarz M, et al. Non-immunogenic dextran-coated superparamagnetic iron oxide nanoparticles: a biocompatible, size-tunable contrast agent for magnetic resonance imaging. *Int J Nanomedicine*. 2017;12:5223–5238. doi:10.2147/IJN.S138108

34. Unterweger H, Dézsi L, Matuszak J, et al. Dextran-coated superparamagnetic iron oxide nanoparticles for magnetic resonance imaging: evaluation of size-dependent imaging properties, storage stability and safety. *Int J Nanomedicine*. 2018;13:1899–1915. doi:10.2147/IJN.S156528

35. Frullano L, Meade TJ. Multimodal MRI contrast agents. *J Biol Inorg Chem*. 2007;12(7):939–949. doi:10.1007/s00775-007-0265-3

36. Munoz LE, Maueroder C, Chaurio R, Berens C, Herrmann M, Janko C. Colourful death: six-parameter classification of cell death by flow cytometry–dead cells tell tales. *Autoimmunity*. 2013;46(5):336–341. doi:10.3109/08916934.2012.755960

37. Alev M, Egenberger L, Mühleisen L, et al. Targeting of drug-loaded nanoparticles to tumor sites increases cell death and release of danger signals. *J Control Release*. 2018;285:67–80. doi:10.1016/j.jconrel.2018.07.007

38. Cossarizza A, Ferraresi R, Troiano L, et al. Simultaneous analysis of reactive oxygen species and reduced glutathione content in living cells by polychromatic flow cytometry. *Nat Protoc*. 2009;4(12):1790–1797. doi:10.1038/nprot.2009.189

39. Szebeni J. Complement activation-related pseudoallergy: a stress reaction in blood triggered by nanomedicines and biologicals. *Mol Immunol*. 2014;61(2):163–173. doi:10.1016/j.molimm.2014.06.038

40. Szebeni J, Fishbane S, Hedenus M, et al. Hypersensitivity to intravenous iron: classification, terminology, mechanisms and management. *Br J Pharmacol*. 2015;172(21):5025–5036. doi:10.1111/bph.13268

41. Kim E, Kim JM, Kim L, et al. The effect of neutral-surface iron oxide nanoparticles on cellular uptake and signaling pathways. *Int J Nanomedicine*. 2016;11:4595–4607. doi:10.2147/IJN.S110332

42. Yilmaz A, Dengler MA, van der Kuip H, et al. Imaging of myocardial infarction using ultrasmall superparamagnetic iron oxide nanoparticles: a human study using a multi-parametric cardiovascular magnetic resonance imaging approach. *Eur Heart J*. 2013;34(6):462–475. doi:10.1093/eurheartj/ehs366

43. Friedrich RP, Janko C, Poettler M, et al. Flow cytometry for intracellular SPION quantification: specificity and sensitivity in comparison with spectroscopic methods. *Int J Nanomedicine*. 2015;10:4185–4201. doi:10.2147/IJN.S82714

44. Weiszhár Z, Czúcz J, Révész C, Rosivall L, Szebeni J, Rozsnyay Z. Complement activation by polyethoxylated pharmaceutical surfactants: Cremophor-EL, Tween-80 and Tween-20. *Eur J Pharm Sci*. 2012;45(4):492–498. doi:10.1016/j.ejps.2011.09.016

45. Szebeni J, Bedocs P, Csukas D, Rosivall L, Bunger R, Urbanics R. A porcine model of complement-mediated infusion reactions to drug carrier nanosystems and other medicines. *Adv Drug Deliv Rev*. 2012;64(15):1706–1716. doi:10.1016/j.addr.2012.07.005

46. Christmann K. Principles of colloid and surface chemistry. *Angew Chem*. 1979;91(1):95–96. doi:10.1002/ange.19790910135

47. Wang YX, Hussain SM, Krestin GP. Superparamagnetic iron oxide contrast agents: physicochemical characteristics and applications in MR imaging. *Eur Radiol*. 2001;11(11):2319–2331. doi:10.1007/s003300100908

48. Rohrer M, Bauer H, Mintorovitch J, Requardt M, Weinmann HJ. Comparison of magnetic properties of MRI contrast media solutions at different magnetic field strengths. *Invest Radiol*. 2005;40(11):715–724. doi:10.1097/01.rli.0000184756.66360.d3

49. de la Harpe KM, Kondiah PPD, Choonara YE, Marimuthu T, du Toit LC, Pillay V. The hemocompatibility of nanoparticles: a review of cell-nanoparticle interactions and hemostasis. *Cells*. 2019;8(10). doi:10.3390/cells8101209

50. Li L, Yan X, Xia M, et al. Nanoparticle/nanocarrier formulation as an antigen: the immunogenicity and antigenicity of itself. *Mol Pharm*. 2022;19 (1):148–159. doi:10.1021/acs.molpharmaceut.1c00704

51. Muñoz LE, Bilyy R, Biermann MHC, et al. Nanoparticles size-dependently initiate self-limiting NETosis-driven inflammation. *Proc Natl Acad Sci*. 2016;113(40):E5856–E5865. doi:10.1073/pnas.1602230113

52. Szebeni J. Complement activation-related pseudoallergy: a new class of drug-induced acute immune toxicity. *Toxicology*. 2005;216(2):106–121. doi:10.1016/j.tox.2005.07.023

53. Mészáros T, Kozma GT, Shimizu T, et al. Involvement of complement activation in the pulmonary vasoactivity of polystyrene nanoparticles in pigs: unique surface properties underlying alternative pathway activation and instant opsonization. *Int J Nanomedicine*. 2018;13:6345–6357. doi:10.2147/IJN.S161369

54. Banda NK, Mehta G, Chao Y, et al. Mechanisms of complement activation by dextran-coated superparamagnetic iron oxide (SPIO) nanoworms in mouse versus human serum. *Part Fibre Toxicol*. 2014;11(64):1–10. doi:10.1186/s12989-014-0064-2

55. Wang G, Chen F, Banda NK, et al. Activation of human complement system by dextran-coated iron oxide nanoparticles is not affected by dextran/ Fe ratio, hydroxyl modifications, and crosslinking. *Front Immunol*. 2016;7:418. doi:10.3389/fimmu.2016.00418

56. Wang G, Inturi S, Serkova NJ, et al. High-relaxivity superparamagnetic iron oxide nanoworms with decreased immune recognition and long-circulating properties. *ACS Nano*. 2014;8(12):12437–12449. doi:10.1021/nn505126b

57. Chao Y, Makale M, Karmali PP, et al. Recognition of dextran-superparamagnetic iron oxide nanoparticle conjugates (Feridex) via macrophage scavenger receptor charged domains. *Bioconjug Chem*. 2012;23(5):1003–1009. doi:10.1021/bc200685a

58. Chao Y, Karmali PP, Mukthavaram R, et al. Direct recognition of superparamagnetic nanocrystals by macrophage scavenger receptor SR-AI. *ACS Nano*. 2013;7(5):4289–4298. doi:10.1021/nn400769e